Design and fabrication of covalently linked PEGylated nanohybrids of ZnO quantum dots with preserved and tunable fluorescence

Article *in* Materials & design · June 2017

DOI: 10.1016/j.matdes.2017.06.019

CITATION
1

READS
174

6 authors, including:

M. S. Salman
UNSW Sydney
8 PUBLICATIONS **9** CITATIONS
SEE PROFILE

Asim Riaz
Australian National University
10 PUBLICATIONS **33** CITATIONS
SEE PROFILE

Azhar Iqbal
Quaid-i-Azam University
12 PUBLICATIONS **22** CITATIONS
SEE PROFILE

Saima Shabbir
Institute of Space Technology
24 PUBLICATIONS **201** CITATIONS
SEE PROFILE

Materials & Design 131 (2017) 156–166

Contents lists available at ScienceDirect

Materials & Design

journal homepage: www.elsevier.com/locate/matdes

Design and fabrication of covalently linked PEGylated nanohybrids of ZnO quantum dots with preserved and tunable fluorescence

Muhammad Saad Salman[a,e,1], Asim Riaz[a,1], Azhar Iqbal[b], Sonia Zulfiqar[c,d], Muhammad Ilyas Sarwar[b,c], Saima Shabbir[a,*]

[a] Department of Materials Science and Engineering, Institute of Space Technology, Islamabad 44000, Pakistan
[b] Department of Chemistry, Quaid-i-Azam University, Islamabad 45320, Pakistan
[c] Department of Chemistry, School of Natural Sciences (SNS), National University of Sciences and Technology (NUST), Islamabad, 44000, Pakistan
[d] Institute for Polymer Materials, POLYMAT, University of the Basque Country (UPV–EHU), Joxe Mari Korta Center, Avda. Tolosa 72, 20018 Donostia-San Sebastian, Spain
[e] School of Chemical Engineering and SKKU Advanced Institute of Nanotechnology (SAINT), Sungkyunkwan University, Suwon 16419, Republic of Korea

ARTICLE INFO

Keywords:
ZnO
Quantum dots
Functionalization
Luminescence
Hydrophilic polymers
Biomarker

ABSTRACT

Non-toxicity, high photo stability, biocompatibility and long lasting narrow emissions are some prime factors for an efficient biological marker. Unfortunately, commercial dyes and Cd-based fluorescent probes do not have such characteristics. Therefore, an efficient fluorescent probe is extremely desirable. Herein, functionalized ZnO quantum dots (QDs) and their nanohybrids with polyethylene glycol (PEG) were prepared by a room temperature solution growth tactic using 3-isocyanatopropyltriethoxysilane (3-ICPTES) as a coupling agent. Isocyanato functional groups were hosted on the surface of as prepared ZnO QDs by introducing optimized stoichiometric amounts of 3-ICPTES. The ZnO QDs were further bonded covalently to PEG via urethane linkages by the reaction of isocyanato functionalized ZnO QDs and hydroxyl groups from PEG molecules. The fluorescence was tuned from cyan to yellowish color after the functionalization of ZnO QDs with 3-ICPTES. Moreover, PEGylated nanohybrids showed greater water dispensability with photoluminescence preserved for at least six months. The present synthesis and coupling strategy for QDs may open up new ways to achieve biocompatible nanohybrids with higher stability and efficient luminescence for bio-imaging and biomedical applications.

GRAPHICAL ABSTRACT

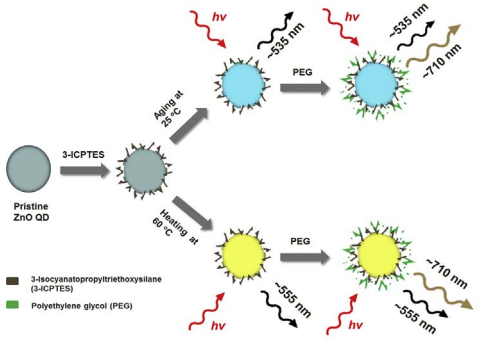

* Corresponding author.
E-mail address: saima.shabbir@ist.edu.pk (S. Shabbir).
[1] These authors contributed equally to this work.

http://dx.doi.org/10.1016/j.matdes.2017.06.019
Received 25 April 2017; Received in revised form 7 June 2017; Accepted 8 June 2017
Available online 09 June 2017

1. Introduction

Quantum dots (QDs) belong to a special class of semiconductor nanomaterials that have garnered great attention in the past few decades owing to their quantum confinement dependent light-driven properties [1]. By virtue of their unique optical properties, they are being used in several applications ranging from optoelectronic devices [1–3] to bioimaging and biosensing areas [4–6]. Particularly, QDs have high photo-stability, narrow emissions, high extinction coefficient and single source excitation, which make them suitable as fluorescence markers for bioimaging applications over the conventional organic fluorophores [4,7]. The prerequisite of QDs, specific to biological applications, is that they should be bio-compatible and water soluble. These properties are affected by their nature, size, charge concentration, outer coating and stability in aqueous medium. Primarily, some QDs are not toxic but they become toxic after the deterioration of outer capping. An important factor contributing towards toxicity is their exposed concentration in vivo, for example Cd based QDs are toxic even at microgram concentrations [8]. Keeping in view the toxicity issues associated with the Cd based QDs, a search for Cd-free and biocompatible semiconductor material has become increasingly important and is the most challenging aspect in biological applications.

ZnO is a promising alternative candidate to Cd based QDs. It has a direct wide band gap of 3.37 eV in the bulk and a large exciton binding energy which makes its exciton stable at room temperature, thus, causing UV emission following exciton recombination [2]. As the emission band of ZnO lies under UV region, therefore, it is used in light-emitting-diode (LED) devices of short wavelengths and even as a replacement for GaN based LEDs. ZnO can also be used in semiconductor lasers and transparent electrodes for solar cells [9]. It is a biocompatible material because of its low level of toxicity which makes it viable for biomedical applications [10]. Essentially, the key features of ZnO that make it imperative and suitable for bio-imaging and cancer detection applications are its biocompatibility, nontoxicity and environment friendliness [6,11].

The major concern in biological applications is that QDs are unstable when they are prepared in aqueous medium and their luminescence diminishes gradually. Therefore, to achieve water solubility and photostability they are required to be surface protected or encapsulated by organic shells, which has been achieved by different surface modification strategies. One of the best strategies to protect QD surfaces is to cap them with an outer shell by a wide band gap semiconductor like silica (SiO_2) [12]. Briefly, the surface of freshly prepared QDs is capped with silane (methoxy or ethoxy) groups; these silanes can be cross-linked to form siloxane linkages. Additionally, many polymer surfaces functionalize by physical adsorption like poly (methyl methacrylate) (PMMA) [13], linear PEG [14], linear poly (alkylamine) (PAL) [15], hyper-branched poly(ethyleneimine) (PEI) [16], polyamidoamine (PAMAM) [17], imidazole functionalized poly (*N*-isopropylacrylamide) (PNIPAM), poly(*N*-vinylcaprolactam) (PVCL) nanogels [18] and chitosan [19]. Capping QD surfaces further prevents other problems like oxidation and deterioration of luminescence properties.

M. Patra et al. [20] employed tetraethyl orthosilicate (TEOS) as a silane capping agent to protect ZnO QD surface with an aim to achieve ZnO QDs with tunable sizes and photoluminescence. Due to a high crosslinking, silica shell originated from TEOS was stable and less toxic. However, it would be noteworthy here that TEOS could only protect the surface but it could not be used to further covalently conjugate with other ligands or polymers intrinsically. To this end, certain coupling agents were proposed for chemical attachment on the functionalized surfaces which could form covalent bonds with various polymers. For instance, PEG with certain oxide ligands was used to bind with QDs thereby generating a biocompatible and chemically stable polymer/QD hybrid which showed efficient luminescence properties [21]. Additionally, numerous efforts were made to demonstrate surface functionalization of QDs either physically or chemically but suitable particle size, water solubility and photostability still remained a goal to be accomplished.

Herein, with the objective to achieve biocompatible, water soluble and photostable ZnO QDs, we report the synthesis of ZnO QDs using 3-isocyanatoproplytriethoxysilane (3-ICPTES) as a capping material. We also demonstrate the fabrication of their PEGylated nanohybrids thus making them biocompatible and water soluble. The sizes of the ZnO QDs were controlled by varying the curing temperature, while the presence of isocyanato functional groups on the ZnO QDs surfaces facilitated the formation of covalent linkages i.e. urethane linkages with hydroxyl groups of PEG molecules. Further, the morphology, photostability, band gap to size variations and associated luminescent properties have been evaluated using several techniques. Particularly, a plausible fluorescence mechanism originating from the organic ligands attached to QDs has been proposed.

2. Experimental

2.1. Materials

The following chemicals were used as received without further purification (unless otherwise specified): zinc acetate dihydrate ($Zn(CH_3COO)_2{\cdot}2H_2O$, BDH, > 99.9%), potassium hydroxide (KOH, Fluka, > 99.9%), methanol (CH_3OH, Fluka, 98%), acetone (CH_3COCH_3, Sigma-Aldrich, ACS reagent, ≥ 99.5%), 3-isocyantopropyletriethoxysilane ($((C_2H_5O)_3Si(CH_2)NCO$, Sigma-Aldrich, 95%), polyethylene glycol (Merck, 8000 $gmol^{-1}$) and demineralized water (DMW). Methanol and acetone were subjected to distillation to remove traces of water thus avoiding reaction of isocyanate groups with moisture.

2.2. Synthesis of ZnO QDs

The synthesis protocol of ZnO QDs reported elsewhere [20] has been executed with minor changes. Briefly, solutions of 0.1 M zinc acetate and 1 M KOH were prepared separately using methanol as a solvent. The reaction was carried out at room temperature by drop wise addition of 1 M KOH to Zn^{2+} solution with constant stirring. The resulting solution was homogenized by stirring continuously for 60 min with the aid of a magnetic stirrer. The solution thus obtained was found to show cyan color luminescence under UV excitation (λ_{exc} 365 nm), thereby, indicating the formation of ZnO QDs. These QDs were recovered by centrifugation (5000 rpm, 5 min, 25 °C) and multiple washings using anhydrous methanol and acetone.

2.3. Surface functionalization of ZnO QDs

For surface functionalization, ZnO QDs were dissolved in anhydrous acetone and an appropriate amount (0.25 mL) of 3-ICPTES was added into the solution (25 mL) to coat and control the growth of ZnO QDs. After several minutes, isocyanate (NCO)-functionalized ZnO QDs were centrifuged (5000 rpm, 5 min, 25 °C) in order to remove unreacted species and NCO functionalized QDs were collected, washed thrice, and re-dissolved in anhydrous acetone again. At this stage, several aliquots were taken for different analyses. Zn—O—Si linkages were formed when ZnO QDs were allowed to react with 3-ICPTES in anhydrous acetone at room temperature (Fig. 1a). For the sake of simplicity, NCO functionalized ZnO QDs aged at room temperature were designated as QD1 and the other sample dried at 60 °C was designated as QD2.

2.4. Fabrication of PEGylated nanohybrids

For a typical synthesis of PEGylated hybrids, stock solutions of 10% PEG (*w/v*) and NCO functionalized ZnO QDs were prepared in anhydrous acetone. Stoichiometric amount of NCO functionalized ZnO QDs was dissolved in appropriate quantities of PEG to get a final

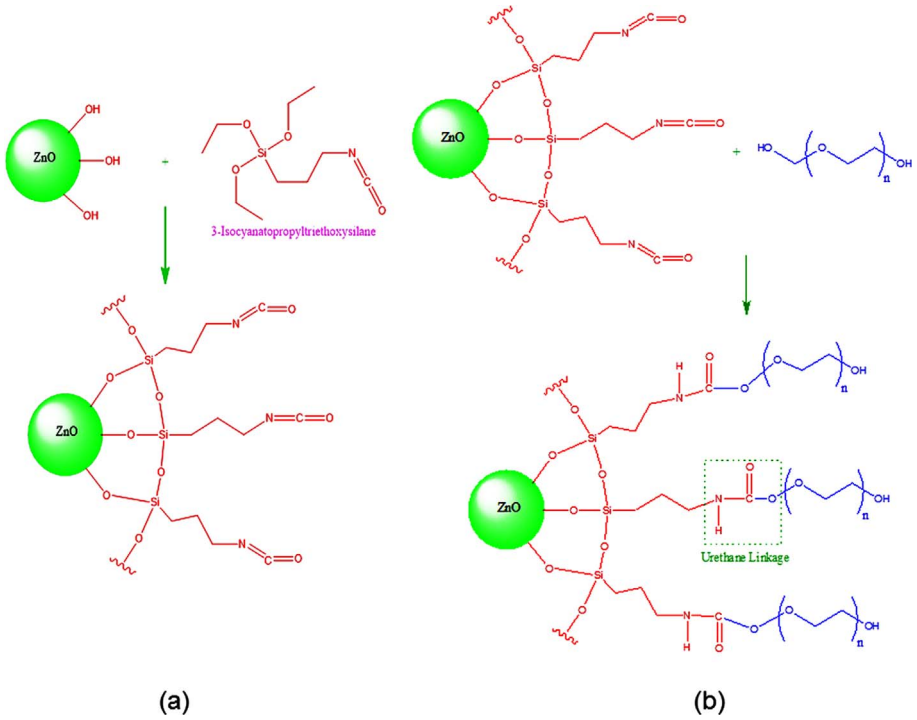

Fig. 1. (a) Scheme for isocyanate functionalization of ZnO QDs and (b) fabrication of PEGylated nanohybrids at room temperature.

concentration of 0.01% *w/v* of ZnO QDs in PEG solution. Then this mixture was allowed to stir magnetically overnight for the completion of the reaction at room temperature. The covalent bonds thus formed, between NCO and PEG, were urethane (—NH—CO—O—) linkages as confirmed by FT-IR spectroscopy. The resultant nanohybrids were collected by centrifuge (5000 rpm, 5 min, 25 °C) in order to remove unreacted molecules and subsequently dispersed in water for storage and further analysis. The nanohybrids fabricated using QD1 and QD2 were designated as H1 and H2, respectively.

2.5. Characterizations

X-ray diffraction (XRD) patterns of powdered samples were obtained by X'pert PRO PANAnalytical X-ray Diffractometer using Ni-filtered Cu Kα radiation (40 kV, 30 mA) with 0.02° steps/s. All the peaks were indexed with PDF# 36-1451. Thermo-Nicolet 6700 FT-IR Spectrophotometer in the range of 400–4000 cm^{-1} was used for functional groups as well as bond analysis at a resolution of 4 cm^{-1}. Atomic Force Microscopy (AFM), model JSPM-5200, in the tapping mode was used for topographical analysis.

For UV–Vis light absorption and band gap estimation, appropriate dilute dispersions were analyzed by Analytik Jena model 205 UV–Vis spectrophotometer in the range of 200 to 800 nm. Emission spectra of different samples were recorded using Labram-3 spectrophotometer manufactured by DongWoo with He–Cd 325 nm laser at room temperature. Field emission scanning electron microscope (FESEM), model MIRA3-XM manufactured by TESCAN, was used to study morphology of QD-PEG nanohybrids. Moreover, the samples were examined on TECNAI G2 20 TWIN (FEI) Transmission Electron Microscope (TEM) operating at an accelerating voltage of 200 kV in a bright-field image mode. Thermal profiles were obtained by NZTECH-429 thermal gravimetric analyzer (TGA) with a ramp of 10 °C/min up to 600 °C in air.

For the fluorescence studies of materials with respect to the response against each excitation wavelength, laser scanning confocal microscopy (LSCM), LSM-510 was used. Nanohybrids were observed on pre-cleaned microscopic glass slide. For this purpose, three types of lasers were used: Ar/Ar-ML 454 nm; Ar/Kr 514 nm and He/Ne 663 nm. Visible color emissions can be demonstrated in any form of the sample, liquid or powder form. In this work, UV lamp source of excitation wavelength (λ_{exc}) 365 nm was used to ascertain the luminescence of as prepared QDs and their PEGylated nanohybrids.

3. Results and discussion

One of the most common ways to validate the presence of QDs is to irradiate them under ultraviolet (UV) light. Therefore, we used UV light source of λ_{exc} 365 nm. Two samples of 3-ICPTES capped ZnO QDs (i.e. QD1 and QD2) were irradiated by UV light source and their resultant luminescence was observed (Fig. 2a). In quantum confinement regime, as the size of the particle increases the band gap tends to decrease. Based on the photon energy–wavelength relation, it can be deduced that bigger particles emit a photon of longer wavelength corresponding to a lesser energy, while smaller sized particles emit photons of high energy with shorter wavelengths. Therefore, it can be stated that QD1 and QD2 samples demonstrated different luminescence results due to their varying sizes and quantum confinement effects (Fig. 2a). Notably, a shift towards the longer wavelength of emitted photon was observed for sample QD2 (Fig. 2a).

Correspondingly, PEGylated nanohybrids (H1 and H2) showed analogous effects under UV irradiation. H1 nanohybrids exhibited cyan color emission (Fig. 2b), validating that H1 nanohybrids contained ZnO QDs of ca. 4–6 nm size. Whereas, H2 nanohybrids demonstrated yellowish color emission, under UV excitation, indicating that H2 comprised of ZnO QDs in the size range of ca. 7–8 nm (Fig. 2b). It is noteworthy here that both the nanohybrids (H1 and H2) can be seen as colorless in the ordinary light (Fig. 2b). Additionally, PEGylated nanohybrids demonstrated a long lasting luminescence for more than six months in water (Fig. 2c). This photostable behavior confirmed the efficient functionalization of QDs by 3-ICPTES at room temperature rendering stable covalent linkages on ZnO QDs with PEG, thereby, inhibiting QDs' growth and preserving their luminescence.

Further, phase purity and particle size estimation of QD1 and QD2 were accomplished by XRD. The typical reflections around 2θ value of 31.60°, 34.50° and 36.25° from the (100), (002) and (101) planes,

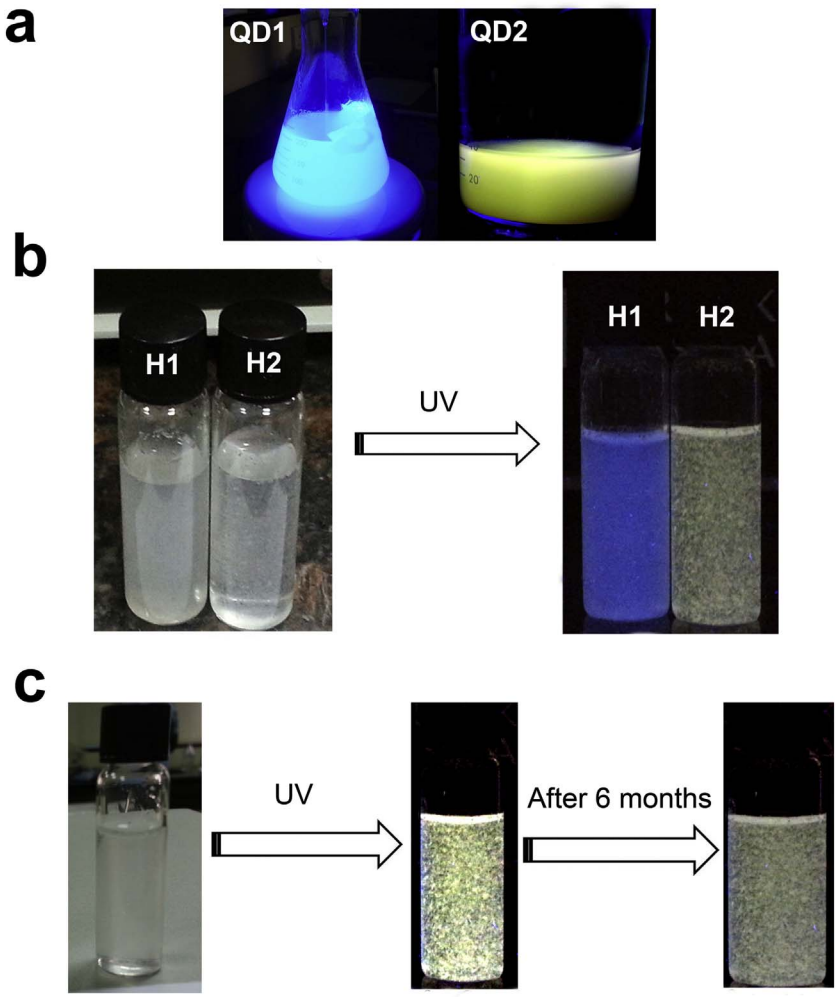

Fig. 2. Luminescence in daylight and under UV of (a) QD1 and QD2, (b) H1 and H2, and (c) photo stability of H2 after six months. (For interpretation of the references to color in this figure, the reader is referred to the web version of this article.)

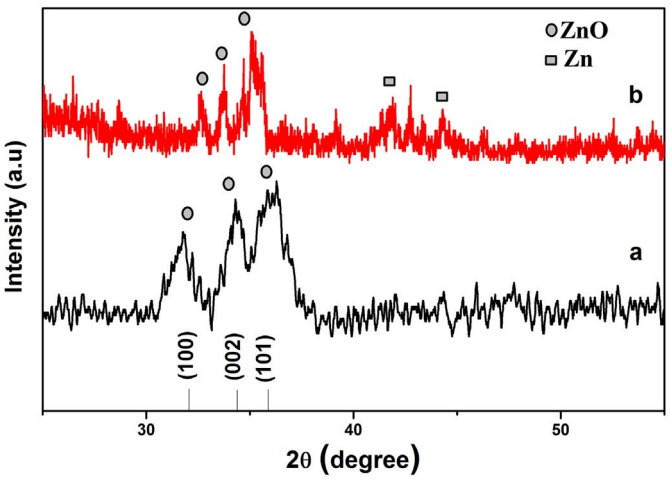

Fig. 3. X-ray diffraction patterns from 25 to 60° of aged and heated samples (a) QD1 and (b) QD2.

respectively were in agreement with the PDF# 36-1451 for polycrystalline wurtzite ZnO [22]. The crystallite sizes of ZnO QDs with XRD patterns shown in Fig. 3 were calculated by Debye Scherer's formula. The average crystallite sizes, determined using (101) plane, were found to be ca. 5 nm and ca. 8 nm for QD1 and QD2, respectively (Fig. 3a, b). Sharper and more intense peaks of QD2 depicted a higher crystallinity and slightly larger crystal size than QD1. The relative higher intensity of QD2 can be attributed to particle growth due to heating at 60 °C, thus, establishing that temperature was an important parameter for controlling the particle size. It is worth mentioning that besides an enhancement in the peak intensity, a peak shift to higher 2θ values was also observed (Fig. 3b). Such a Bragg peak shifting could be credited to the tensile or compressive stresses, where the latter may decrease the d-spacing thus resulting in the peak shift to higher angles [23]. Here, it would be unambiguous if we attribute annealing temperature as the major factor for a peak shift in Fig. 3b. Further, the smaller peaks (background scattering) in the XRD pattern might be attributed to polymer/SiO_2 network originating from 3-ICPTES capped ZnO QDs, therefore, only the most prominent peaks were labeled (Fig. 3).

FT-IR spectra of −NCO-functionalized ZnO QDs (QD1 and QD2) and their respective nanohybrids (H1 and H2) are displayed in Fig. 4. The characteristic band for Zn−O stretching vibrations [24], in all the samples (QD1, QD2, H1 and H2), was shifted to a lower wavenumber of 447 cm^{-1} due to the presence of silica (−Si−O−Si−) network on the ZnO QDs, while Zn−O−Si and Si−OH stretching vibrations appeared at 840 and 890 cm^{-1}, respectively [25]. The presence of Si−OH band confirmed the reaction of 3-ICPTES coupling agent with ZnO QDs to

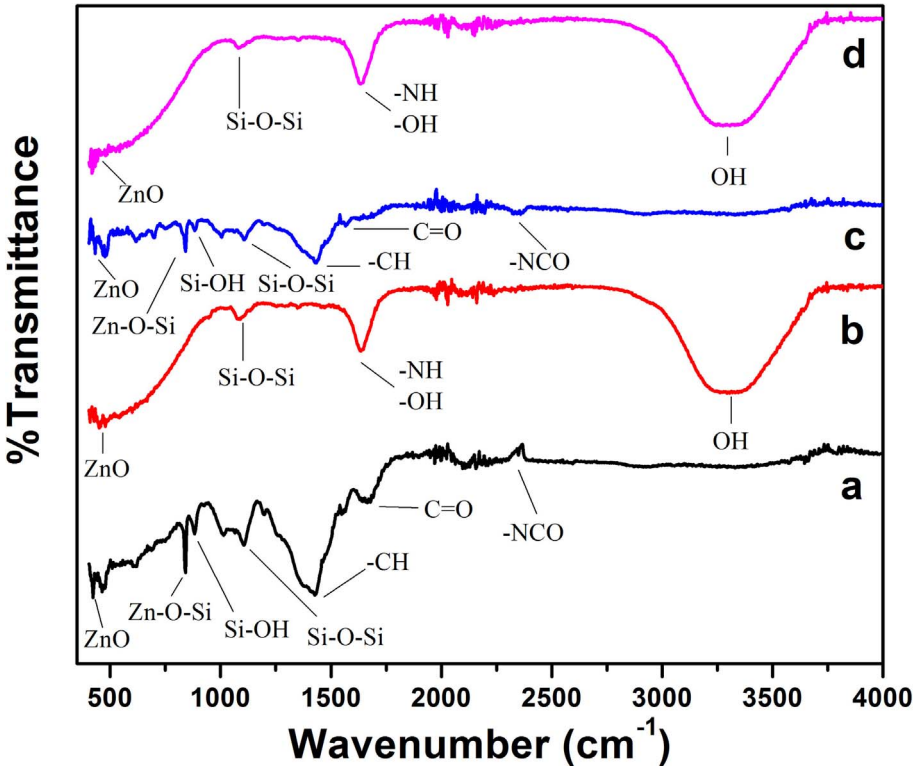

Fig. 4. FT-IR spectra of (a) QD1, (b) H1, (c) QD2 and (d) H2.

form NCO functionalized QD1 and QD2 (Fig. 4a, c), however, Si—OH band was absent in the case of nanohybrid samples H1 and H2 (Fig. 4b, d). After 3-ICPTES capping on ZnO QDs, all the samples showed a band for silica network which was observed around 1080 cm^{-1} due to the bending vibrations of Si—O—Si bonds (Fig. 3b). The bands between 1650 and 1750 cm^{-1} were attributed to urethane C=O stretching vibrations. Moreover, the band at 3436 cm^{-1} was observed, in nanohybrid samples (Fig. 4b, d), due to O—H stretching vibrations while their

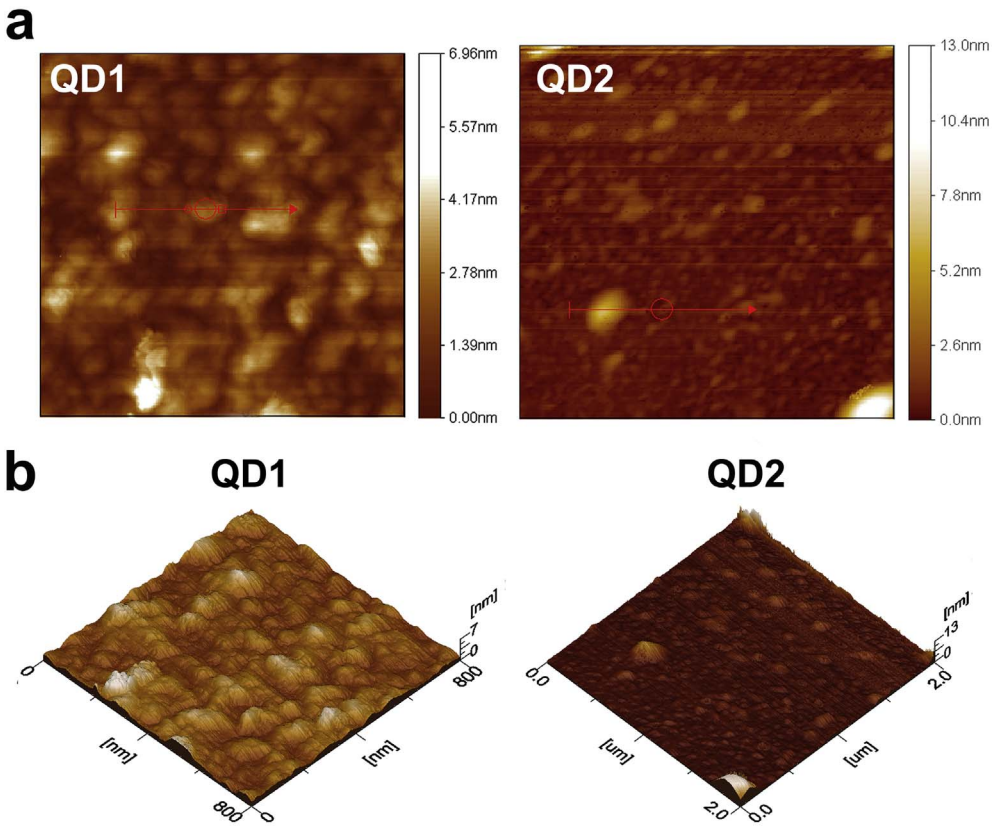

Fig. 5. AFM images of QD1 and QD2 showing (a) 2D topography and (b) 3D topography (800 nm × 7 nm and 2 μm × 13 nm for QD1 and QD2, respectively).

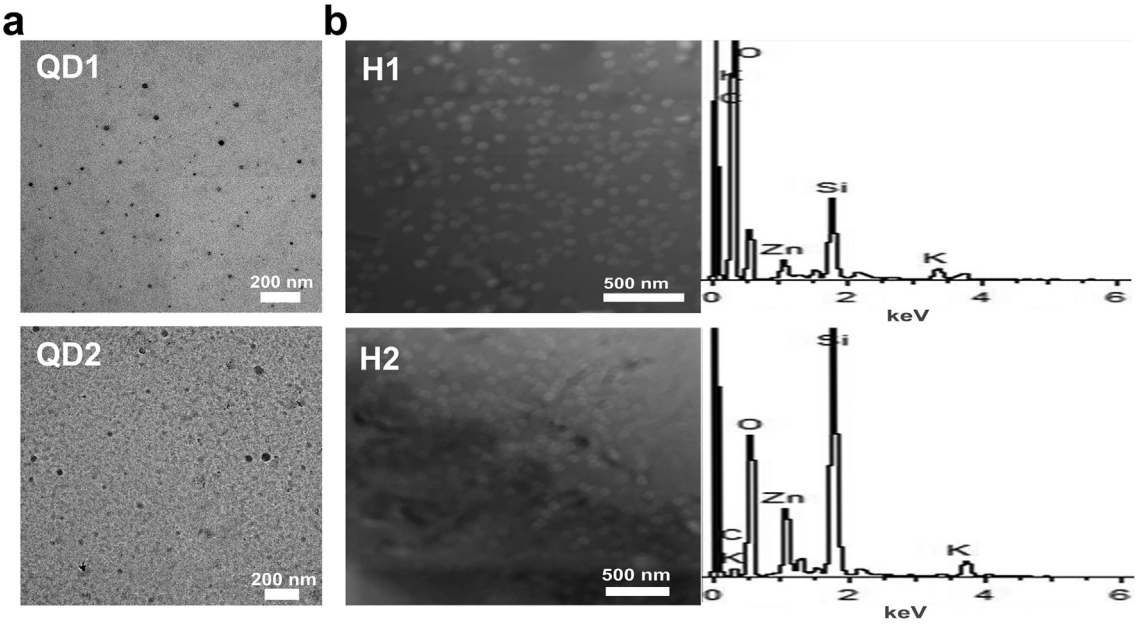

Fig. 6. TEM images of (a) QD1 and QD2 (scale bar: 200 nm) and FESEM images (b) H1 and H2 (scale bar: 500 nm) along with EDS indicating C, K, O, Zn and Si elements.

Table 1
Calculation for grafting efficiency of isocyanate and PEG onto ZnO QDs.

Sample[a]	
NCO (%) (A/B) × 100	
QD1	63
QD2	66
PEGylation efficiency (%) (A/C) × 100	
H1	68.5
H2	78.3

A = weight of grafted polymer, B = weight of inorganic content, C = total weight of polymer and particle.
[a] Initial weight loaded ca. 3.1 mg (all samples) in TGA.

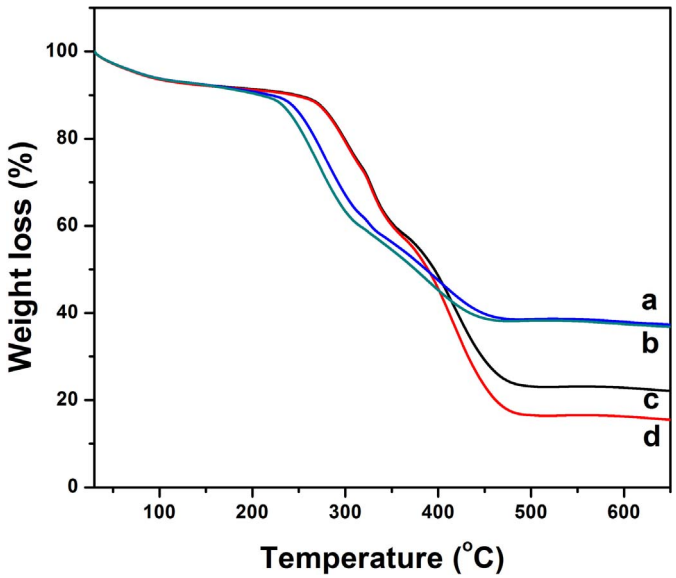

Fig. 7. TGA thermograms of ZnO QDs before and after PEG grafting: (a) QD1, (b) QD2, (c) H1 and (d) H2.

relevant bending vibrations were confirmed by the bands around 1540 cm^{-1} [24].

Moreover, one of the most important and characteristic bands (Fig. 4a, c) was observed around 2270 cm^{-1} in QD1 and QD2. This was attributed to the presence of −N═C═O functional groups that were introduced on the surface of ZnO QDs by the reaction with 3-ICPTES coupling agent. However, it should be noted that FTIR peak for NCO group is not sharp since very little amount of the isocyanate was used as the coupling agent. This −NCO functionality at QD1 and QD2 was covalently bonded with the hydroxyl end groups of PEG thus leading to the formation of nanohybrids via PEGylation of QDs. When the reaction of −OH functional groups of PEG occurred with the −NCO moieties on QDs, it led to the formation of urethane linkages with the ensuing QD/PEG nanohybrids. Therefore, −NCO band around 2270 cm^{-1}, for 3-ICPTES capped ZnO QDs, disappeared (Fig. 4d) after the formation of nanohybrids, thereby, confirming the successful formation of the nanohybrids through urethane linkages (Fig. 1b). Finally, the formation of urethane bonds was ascertained by the suppression of isocyanate band and the appearance of the urethane C═O stretching vibration around 1700 cm^{-1} [26]. Overall, FT-IR results confirmed the proposed synthetic schemes (Fig. 1).

Topographical analysis along with the particle approximation was done using the atomic force microscopy (AFM). Using the tapping mode, 2D AFM surface morphology of QD1 and QD2 is displayed in Fig. 5a. Note, the particle sizes in Fig. 5 are not uniform and the height distributions of QD1 and QD2 are below 7 and 13 nm (Fig. 5a), respectively. The relevant 3D surface illustrations are depicted in Fig. 5b. It was observed that particles were not exactly distinguishable as spherical in AFM which could be due to the tip force and broadening effect. It could also be due to the formation of polymeric network or crosslinking upon drying prior to the analysis. In conjunction to the AFM results, TEM results also showed that the particle sizes of QD1 and QD2 varied with temperature as expected (Fig. 6a); however, their morphologies were essentially spherical with particle sizes of around 4 nm for QD1 and 6 nm for QD2 (bigger size particles were seen in TEM which could be due the coalescence). Further analysis of the nanohybrids by FESEM showed that the nanohybrids were successfully prepared and their sizes were around 30 to 40 nm for H1 and H2 (Fig. 6b), respectively with nearly spherical shapes.

The energy dispersive X-ray spectroscopy (EDS) showed well-defined elemental traces from the precursors (Fig. 6b) and an increase in the nanohybrid size was due to the corresponding increment in the diameter of ZnO QDs as a result of heating [27]. Moreover, it was observed that isocyanate contents largely varied with the particle size of

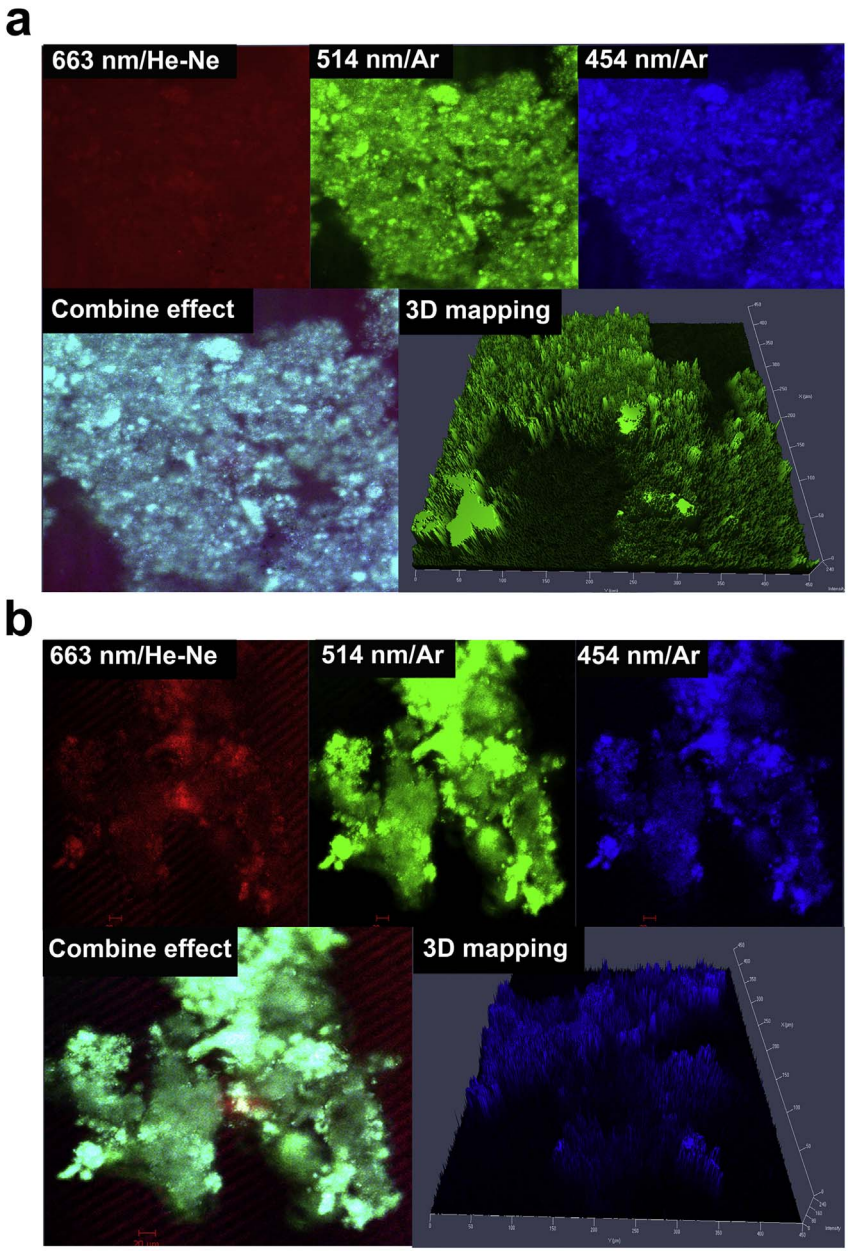

Fig. 8. Confocal laser scanning images showing fluorescence of (a) H1 and (b) H2. (For interpretation of the references to color in this figure, the reader is referred to the web version of this article.)

ZnO QDs due to which Fig. 6b indicated higher silicon content in QD2 than QD1. This may be ascribed to the larger particle size of QD2 having more surfaces for capturing NCO groups as evident from the following TGA evaluation (Fig. 6). From the TGA, the percentage content of the functional groups on ZnO QD surface as well as the PEGylation efficiency in terms of grafting was calculated using a method reported elsewhere [28]. The polymer grafting calculations are listed in Table 1. The weight of the grafted polymers and residue (e.g., ZnO particle) was estimated using TGA (Fig. 7). As depicted in Table 1, QD1 had at least 63% NCO content on its surface (Fig. 7a), whereas, QD2 being larger in size than QD1, hosted higher NCO content than QD1. Hence, ca. 66% NCO was found in the case of QD2 which was in agreement with our expectation (Fig. 7b), while H1 (Fig. 7c) and H2 (Fig. 7d) showed 68.5% and 78.3% PEGylation efficiencies, respectively (Table 1).

FESEM results also revealed that the covalent linkages formed between isocyanate of 3-ICPTES and OH functional groups of PEG restricted the particle agglomeration, thus, making a fine dispersion. The low agglomeration was a result of PEGylation where PEG due to its entropic-repulsions induced dispersed nanohybrids [29]. As-prepared ZnO QDs possess high surface energies that cause a greater tendency to aggregate. For spherical shaped ZnO QDs particles, it is assumed that the interaction potential is related to electrostatic repulsion and weak Van der Waals attractions between the particles. But grafting of PEG tends to decrease the surface free energies of ZnO QDs leading to the minimization of even weak forces like Van der Waals attractions. Therefore, such kinds of entropic-repulsions could specifically be associated with PEG as reported previously by Bertrand et al. [30]. Additionally, it can be deduced from Table 1 that PEGylated ZnO QDs were dispersed in water effectively after PEGylation (Fig. 6b).

After the successful fabrication of the nanohybrids we investigated their fluorescence by confocal microscopy. Fluorescence images of freshly prepared (non-agitated and without sonication) H1 and H2 nanohybrids of ZnO QDs are shown in Fig. 8. Three excitation

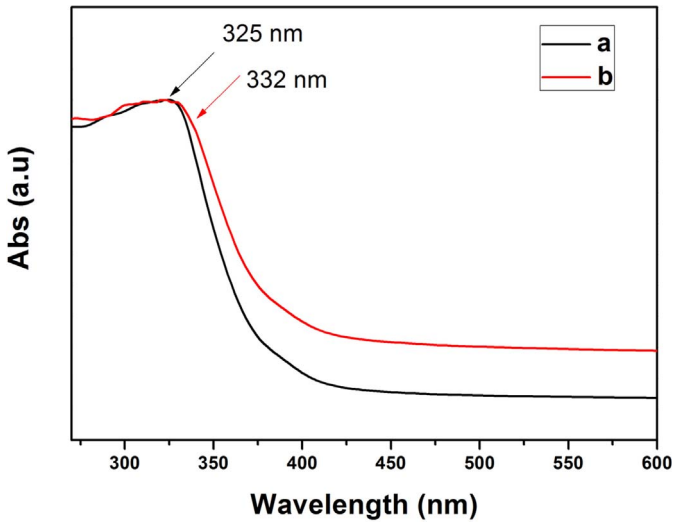

Fig. 9. UV-Vis spectra of (a) QD1 (b) QD2 from 200 to 600 nm at room temperature.

wavelengths obtained by lasers were used to monitor fluorescence following excitation in the hybrid samples. The fluorescence intensity of H1 nanohybrid varied with the excitation wavelength of the lasers and its fluorescence was very high between 454 and 514 nm range (Fig. 8a). The combined (overlay) image, as shown in Fig. 8a, clearly exhibited the fluorescence (cyan color) by H1. With the longer excitation wavelength of laser the fluorescence intensity was low and by decreasing the wavelength from 532 to 454 nm the fluorescence increased. Further, the overlay of fluorescence of H2 nanohybrid by all three lasers is shown in Fig. 8b. Here also, the combined (overlay) image, as shown in Fig. 8b, exhibited green-yellowish fluorescence by H2. Overall, the fluorescence results shown in Fig. 8 can be corroborated well with the results in Fig. 2.

Moreover, Fig. 9 illustrates the optical absorption spectra of ZnO QDs dispersed in ethanol at room temperature. The absorption wavelengths were ca. 325 and 332 nm for QD1 and QD2, respectively (Fig. 9a, b). The band edge onset was blue shifted for QD1 due to reduction in the particle size to ca. 4 nm and the quantum confinement effect, whereas, the increment in QD2 particle size was due to heating at 60 °C (Fig. 9b) [27] and had a smaller band gap of 3.57 eV than 3.8 eV of QD1. The band gap of ZnO QDs has been calculated by Eq. 1, where the band gap depends on the particle size [31].

$$E_g^* = E_E^{bulk} + \left[\left(\frac{h^2}{8R^2}\right) \times \left(\frac{1}{m_e} + \frac{1}{m_h}\right) - \left(\frac{1.8e^2}{4\pi\varepsilon_0\varepsilon_r R}\right)\right] \quad (1)$$

In Eq. 1, E_g^{bulk} is the band gap energy of bulk ZnO i.e. 3.37 eV [32], E_g^* is band gap energy of ZnO QDs, h is the Planck's constant, R is particle radius, ε is dielectric constant for material, m_h is effective mass of hole and m_e is the effective mass of electron. For ZnO, ε is 8.5, $m_e = 0.26\ m_o$ and $m_h = 0.59\ m_o$ [33]. In addition, it was anticipated that the capping agent also played an important role in varying the band gaps. For instance, ZnO nanoparticles capped with TEOS had a band gap of 3.67 eV but in our case 3-ICPTES showed an increase in the band gap, even though all the parameters were kept constant [20]. Therefore, it indicated suppression in Ostwald ripening of ZnO QDs upon surface functionalization by 3-ICPTES. Further, in another study, ZnO capped with 2-hydroxypropionic acid (HPA) showed a band gap of 3.52 eV [34] which was also lower than the ZnO QDs in the present study.

In conjunction with the aforementioned band gap calculation, we also estimated the possible band gap dependent absorption and emissions from ZnO QDs. The absorption values estimated by the photon energy–wavelength relation based on the particle sizes were found to be

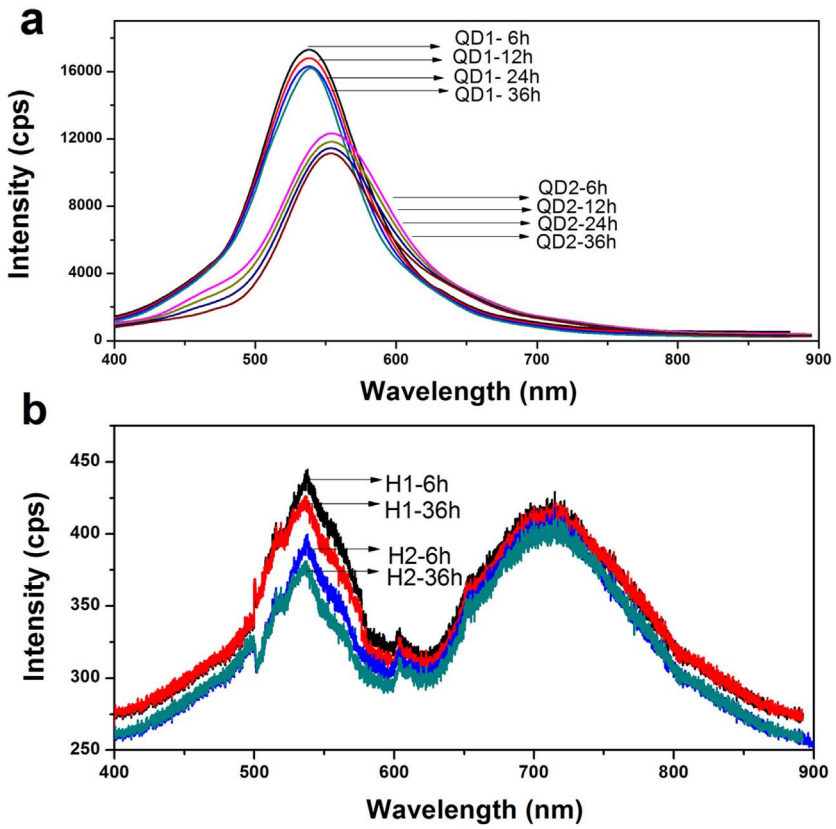

Fig. 10. The room temperature PL spectra showing emission in visible regions (a) QD1, QD2, and (b) H1, H2. (For interpretation of the references to color in this figure, the reader is referred to the web version of this article.)

ca. 326 and 340 nm for QD1 and QD2, respectively. The calculated band-edge absorptions and energy values for ZnO QDs were quite close to and in agreement with the UV absorbance results in Fig. 9. Further, the emission spectra of QD1, QD2 and their nanohybrids (H1 and H2) at different time intervals were investigated as shown in Fig. 10. QD1 showed a narrower and intense peak near 535 nm, whereas QD2 showed relatively broader and less intense peak around ca. 555 nm. To elucidate the plausible cause behind these emissions, we tried to correlate the band gap widening or shrinking to the luminescence shown in Fig. 10. As elaborated earlier, ZnO QDs exhibited quantum size effects, broad band gaps and the red shifts in the emissions from 535 to 555 nm. Therefore, it must be kept in mind that the band gap dependent emissions from ZnO QDs usually show UV to bluish color with the emission wavelengths in the range of ca. 400–450 nm. Conversely, the emissions from the ZnO QDs in the present work fall under the cyan and green-yellowish color regime, probably originating from defect states rather than from the band gaps intrinsically.

In order to validate this hypothesis, we explored the cause of the visible emissions from ZnO in the already reported works [35,36] and found that different intrinsic defects [37,38] such as zinc vacancy (V_{zn}), zinc interstitial (Zn_i), oxygen vacancy (V_o^*), oxygen interstitial (O_i), antisite oxygen (O_{zn}) and extrinsic one like impurities e.g., metallic-ion defect centers were responsible for the emissions [39–41]. However, the contribution of these defects in the emission band is still not well understood [39,42,43]. Meanwhile, the emission band of ZnO QDs by the recombination of exciton was due to the singly-ionized oxygen vacancies [44]. It was reported that when the photo generated holes, trapped in deep levels inside the band gap of ZnO particles, recombine radiatively with the electron occupying the oxygen vacancy, emission was produced [33]. The trapping of holes increased with decreasing particle size due to increase in surface-to-volume ratio that caused the emission in visible region [45,46]. As the particle size increased its band gap decreased so that the exciton recombination took place in a narrower energy gap, hence, generating emission of higher wavelength and vice versa. Although, the variation in the band gap altered the emissions in ZnO QDs, it was only a minor part. Therefore, it is anticipated that the visible emissions from ZnO QDs originated from the defects on the surfaces [20]. Our hypothesis for the visible emissions in this study is also consistent with the previous work, where ZnO nanoparticles exhibited strong yellow emissions resulting from defects possibly from singly-ionized oxygen vacancies [47].

Notably, changes in the PL emissions intensity can be seen in Fig. 10. It can be effectively explained by considering the size [33] and surface states of QDs [48,49], therefore, both were considered while studying optical properties of QDs along with other parameters. For instance, the particle sizes were tuned by curing temperatures, herein, resulting in different absorption and emission profiles. Further, the capping agent protected the surface of the ZnO QDs and showed great influence on reducing the probability of agglomeration of particles depending upon the storage condition. With an aim to study the effect of capping material on luminescence, previously, the PL intensity dependence on ZnO QDs size and stability was investigated with several silane coupling agents [20,50]. Polyether-grafted ZnO QDs incorporating different silanes like 3-aminopropyltrimethoxysilane (APTMS) and 3-(2,3-(epoxypropoxy)propyl) trimethoxysilane coupling agents displayed better stability, than the unmodified ZnO QDs, and capped QDs remained stable for 9 weeks in comparison to 15 days for unmodified QDs. This confirms that surface modification can considerably enhance both the luminescence as well as the stability of ZnO QDs in water. Here, when temperature was increased to 60 °C for QD2 (Fig. 10a), reduced intensity of emission was observed. Therefore, we anticipate that the reduction in the intensity could be due to increase in the particle size, agglomeration and degradation of 3-ICPTES cross-linking/network. The photoluminescence at time intervals from 6 to 36 h in the present study showed a typical decrease in intensity, consistent with the study by M.K. Patra [20]. Accordingly, the effect of particle growth on intensity seemed reasonable as there were small red shifts in the luminescence spectra for the period of 6 to 36 h from 535 to 540 nm and 555 to 559 nm for QD1 and QD2, respectively (Fig. 10a).

Further, it has been observed that 3-ICPTES helped to reduce the particle size and particle growth that in turn optimized efficient capping on ZnO QDs [48,51]. Previously, the effect of HPA on the optical properties of ZnO was studied, in which HPA coated ZnO in $CHCl_3$ showed multiple emissions at 353 (bluish color) and 515 nm (green-yellowish color) [34]. Besides, ZnO QDs with yellow emissions prepared often by thermal treatment of green-emitting ZnO QDs exhibited 20% lower quantum yields (QYs) than blue emitting ZnO QDs [50]. This was similar to the trend observed in the present study because as the particle size of ZnO QDs increased, in the case of yellow color emitting QD2 (Fig. 10a), their luminescence intensity decreased. Correspondingly, photostability of ZnO QDs was also reduced due to heat treatment [27]. This could also be associated with the electron-hole trapping phenomenon on the QDs' surfaces where an increase in particle size upon heating led to the reduction in the electron mobility from the conduction band as explained earlier.

Among several other reasons, the direct polymer capping on ZnO QDs is one of the primary factors for the reduction of luminescence [52]. This was also studied by Abdullah et al. who synthesized PEG protected ZnO nanoparticles through an in situ method [53]. Therefore, mixing of polymers with the ZnO QDs has not been widely accepted as an effective procedure to preserve or enhance the luminescence of ZnO QDs. Thus, in the present approach, this problem has been addressed through the surface functionalization of ZnO QDs with 3-ICPTES which can protect and even improve their luminescence properties via PEG grafting. Upon PEGylation, the structures of the PEGylated nanohybrids i.e. H1 and H2 were covalently held by urethane linkages. It is noteworthy here that our present tactic for the covalent linkage of polymers on the ZnO QDs is a convenient alternative, especially in the context of the bioconjugation for biological applications [54]. Moreover, the luminescence characteristics of H1 and H2 at different time intervals were studied and the results are shown in Fig. 10b. Notably, the luminescence intensity of H1 and H2 was lower than the original intensity of QD1 and QD2 (Fig. 10a). This could be attributed to PEGylation [55] on functionalized ZnO QDs which led to the decreased intensity due to the reduction in specific luminescence sites on ZnO QDs as well as the size increment. However, the decrease in intensity was not that much significant even after 3 weeks of storage at room temperature.

In comparison to the present study, synthesis of ZnO nanoparticles was reported by the reaction between zinc acetate and KOH in methanol. Furthermore, ZnO-(PEGMA) fabrication was done by the polymerization on ZnO particles but the final product did not show any luminescence [56]. Though the samples were well crystalline, as analyzed by XRD, the reason for non-luminescent ZnO-(PEGMA) might be the absence of defects and related emissions in the spectra. From this it can be strongly deduced that in Fig. 10 the visible luminescence of the particles was associated with the surface defect states on the QDs which decreased as the particles grow. Hence, a decrease in the intensity occurred significantly and then after reaching a saturation point it decreased as a function of time. Additionally, in comparison to our choice of 3-ICPTES, some other capping agents [57] were also previously used for surface functionalization of ZnO such as: APTMS, TEOS and mercaptosuccinic acid (Ms) which were found good in growth suppression of particles whereas others namely: 3-mercaptopropyl trimethoxysilane (Mp) and polyvinylpyrrolidone (PVP) were not effective in capping, and led to the agglomeration of particles. The stability analysis of previously studied QDs confirmed them to be stable up to six weeks with a growth in the range of 100–500 nm in diameter during this duration. It is significant here that size of the particle exceeding ~100 nm limited their use in biological applications. In this regard, present work on 3-ICPTES capped ZnO-QDs and their PEGylated nanohybrids with sizes < 100 nm showed stable luminescence up to six months in water (Fig. 2), especially as compared to TEOS capped ZnO QDs which showed

90 days of stability [20] with the parallel synthesis procedure. Hence, the present approach makes them conducive for several biological applications. This led to an important inference that 3-ICPTES was a valuable addition to all previously reported silane coupling agents, since it is an effective growth suppressor, an efficient linker and a cause of steric hindrance to −Si−O−Si− network in ZnO QDs.

Particularly after PEGylation, it is interesting to see that even the luminescence from the ZnO QDs ca. 530 to 555 nm still appeared (Fig. 10b) though its intensity was decreased. In order to investigate the underlying phenomenon; we compared the results with and without PEGylation. The photoluminescence from ZnO QDs (Fig. 10a) showed that before the PEGylation, intensity was much higher as compared to after PEGylation and there was no additional peak in the red region. This could be explained in two ways; one being the PEGylation efficiency and the other reduction in the intensity. Fig. 10b shows that approximately 37-fold reduction in the PL intensity was observed in the PEGylated samples (i.e. 450 cps) as compared to ZnO QDs (i.e. 17,000 cps). The reduction in the PL intensity in the present work is consistent with previously reported works where PEG led to the reduction in the intensity by suppressing the defect states responsible for high intensity emission [55]. Fig. 10 further confirmed that PEG was successfully linked with functionalized ZnO QDs leading to the reduction in the intensity; hence, PEGylation also influenced the QDs' luminescence. Additionally, the peaks appearing ca. 710 nm in all the hybrid samples (Fig. 10b) at different time intervals could be ascribed to second order light scattering piling up on the detector or may just be an artefact as described by Tachikawa [58]. However, in order to understand the concept behind this, in our opinion, besides second order scattering phenomenon or instrumental error there could be a true emission coming from the organic–inorganic interfaces as polymers like PEG can absorb light, though they do not exhibit an intrinsic luminescence [59].

Overall, we propose a plausible mechanism behind the unusual 'organo-fluorescence' originating from the organic–inorganic interfaces in nanohybrids. It was surprising to note that wavelength in the visible region was observed which might be due to the hindrance created by polymers (PEG units or urethane) thereby lowering the photon energy; thus, a wavelength in the visible region was detected. As it is well known that emission wavelengths will always be larger than excitation because of energy difference (Stokes shift) so when a light (photon energy) was absorbed by PEGylated ZnO QDs, the electrons from ZnO sites may go to their 'excited state' and then in a similar manner incoming photons may lead to multiple excitation processes on ZnO QDs' surface or organic–inorganic interfaces [60]. Hence, there might be an energy transfer process from ZnO surface to PEG or vice versa which could absorb the incoming photons. However, energy coming out in the form of 'emission' was lowered by polymer chains and resulted in an emission wavelength of ca. 700 nm. Nevertheless, it is anticipated that this special type of fluorescence might be originating from the ZnO–PEG interfaces. In either case, the exact mechanism of such an astonishing organo-luminescence is still not well understood and needs further investigations.

4. Conclusions

In summary, we have successfully synthesized 3-ICPTES functionalized, photostable, water dispersible, biocompatible, cadmium and selenium free, ZnO QDs. The size and luminescence of the functionalized ZnO QDs were varied with curing temperature. Their nanohybrids with urethane covalent linkages were successfully fabricated by the reaction between isocyanato functional groups of 3-ICPTES and hydroxyl groups of PEG at room temperature. Moreover, cyan to yellowish emitting ZnO QDs along with their nanohybrids showed photo-stability for at least six months making them the stable biocompatible markers for long-lasting bio-imaging applications. We believe that our functionalization strategy can be embraced as a reference to obtain various organic–inorganic nanomaterials for biological applications.

Acknowledgement

S. Shabbir acknowledges the Higher Education Commission, Pakistan for funding under the National Research Programme for Universities (20-4023/R & D/HEC/14/345).

References

[1] C.R. Kagan, E. Lifshitz, E.H. Sargent, D.V. Talapin, Building devices from colloidal quantum dots, Science 353 (2016) (aac5523).
[2] U. Ozgur, Y.I. Alivov, C. Liu, A. Teke, M.A. Reshchikov, S. Dogan, V. Avrutin, S.J. Cho, H. Morkoc, A comprehensive review of ZnO materials and devices, J. Appl. Phys. 98 (2005) 041301–041403.
[3] X.M. Li, M.C. Rui, J.Z. Song, Z.H. Shen, H.B. Zeng, Carbon and graphene quantum dots for optoelectronic and energy devices: a review, Adv. Funct. Mater. 25 (2015) 4929–4947.
[4] Y. Wang, R. Hu, G. Lin, I. Roy, K.T. Yong, Functionalized quantum dots for biosensing and bioimaging and concerns on toxicity, ACS Appl. Mater. Interfaces 5 (2013) 2786–2799.
[5] S.J. Xu, D. Li, P.Y. Wu, One-pot, facile, and versatile synthesis of monolayer MoS_2/WS_2 quantum dots as bioimaging probes and efficient electrocatalysts for hydrogen evolution reaction, Adv. Funct. Mater. 25 (2015) 1127–1136.
[6] P. Zhu, Z. Weng, X. Li, X. Liu, S. Wu, K.W.K. Yeung, X. Wang, Z. Cui, X. Yang, P.K. Chu, Biomedical applications of functionalized ZnO nanomaterials: from biosensors to bioimaging, Adv. Mater. Interfaces 3 (2016) 1500494.
[7] J. Zhou, Y. Yang, C.Y. Zhang, Toward biocompatible semiconductor quantum dots: from biosynthesis and bioconjugation to biomedical application, Chem. Rev. 115 (2015) 11669–11717.
[8] R. Hardman, A toxicologic review of quantum dots: toxicity depends on physicochemical and environmental factors, Environ. Health Perspect. 114 (2006) 165–172.
[9] C. Battaglia, J. Escarre, K. Soderstrom, M. Charriere, M. Despeisse, F.J. Haug, C. Ballif, Nanomoulding of transparent zinc oxide electrodes for efficient light trapping in solar cells, Nat. Photonics 5 (2011) 535–538.
[10] J. Zhou, N.S. Xu, Z.L. Wang, Dissolving behavior and stability of ZnO wires in biofluids: a study on biodegradability and biocompatibility of ZnO nanostructures, Adv. Mater. 18 (2006) 2432–2435.
[11] M. Ying-Ying, D. Hui, X. Huan-Ming, Folic acid functionalized ZnO quantum dots for targeted cancer cell imaging, Nanotechnology 26 (2015) 305702.
[12] P. Mulvaney, L.M. Liz-Marzan, M. Giersig, T. Ung, Silica encapsulation of quantum dots and metal clusters, J. Mater. Chem. 10 (2000) 1259–1270.
[13] S.C. Farmer, T.E. Patten, Photoluminescent polymer/quantum dot composite nanoparticles, Chem. Mater. 13 (2001) 3920–3926.
[14] W. Liu, A.B. Greytak, J. Lee, C.R. Wong, J. Park, L.F. Marshall, W. Jiang, P.N. Curtin, A.Y. Ting, D.G. Nocera, D. Fukumura, R.K. Jain, M.G. Bawendi, Compact biocompatible quantum dots via RAFT-mediated synthesis of imidazole-based random copolymer ligand, J. Am. Chem. Soc. 132 (2010) 472–483.
[15] J. Lee, B. Yang, R. Li, T.A. Seery, F. Papadimitrakopoulos, Poly(allylamine)-encapsulated water-soluble CdSe nanocrystals, J. Phys. Chem. B 111 (2007) 81–87.
[16] T. Nann, Phase-transfer of CdSe@ZnS quantum dots using amphiphilic hyperbranched polyethylenimine, Chem. Commun. (2005) 1735–1736.
[17] C.X. Zhang, S. O'Brien, L. Balogh, Comparison and stability of CdSe nanocrystals covered with amphiphilic poly(amidoamine) dendrimers, J. Phys. Chem. B 106 (2002) 10316–10321.
[18] L. Shen, A. Pich, D. Fava, M.F. Wang, S. Kumar, C. Wu, G.D. Scholes, M.A. Winnik, Loading quantum dots into thermo-responsive microgels by reversible transfer from organic solvents to water, J. Mater. Chem. 18 (2008) 763–770.
[19] W.B. Tan, Y. Zhang, Surface modification of gold and quantum dot nanoparticles with chitosan for bioapplications, J. Biomed. Mater. Res., Part A 75 (2005) 56–62.
[20] M.K. Patra, M. Manoth, V.K. Singh, G.S. Gowd, V.S. Choudhry, S.R. Vadera, N. Kumar, Synthesis of stable dispersion of ZnO quantum dots in aqueous medium showing visible emission from bluish green to yellow, J. Lumin. 129 (2009) 320–324.
[21] S.W. Kim, S. Kim, J.B. Tracy, A. Jasanoff, M.G. Bawendi, Phosphine oxide polymer for water-soluble nanoparticles, J. Am. Chem. Soc. 127 (2005) 4556–4557.
[22] P.K. Sharma, R.K. Dutta, M. Kumar, P.K. Singh, A.C. Pandey, Luminescence studies and formation mechanism of symmetrically dispersed ZnO quantum dots embedded in SiO_2 matrix, J. Lumin. 129 (2009) 605–610.
[23] S. Kumar, K. Asokan, R.K. Singh, S. Chatterjee, D. Kanjilal, A.K. Ghosh, Investigations on structural and optical properties of ZnO and ZnO:Co nanoparticles under dense electronic excitations, RSC Adv. 4 (2014) 62123–62131.
[24] L.P. Bauermann, J. Bill, F. Aldinger, Bio-friendly synthesis of ZnO nanoparticles in aqueous solution at near-neutral pH and low temperature, J. Phys. Chem. B 110 (2006) 5182–5185.
[25] C.H. Hung, W.T. Whang, Effect of surface stabilization of nanoparticles on luminescent characteristics in ZnO/poly(hydroxyethyl methacrylate) nanohybrid films, J. Mater. Chem. 15 (2005) 267–274.
[26] I.V. Berlinova, I.V. Dimitrov, R.G. Kalinova, N.G. Vladimirov, Synthesis and aqueous solution behaviour of copolymers containing sulfobetaine moieties in side chains, Polymer 41 (2000) 831–837.
[27] T. Omata, K. Takahashi, S. Hashimoto, Y. Maeda, K. Nose, S. Otsuka-Yao-Matsuo,

K. Kanaori, UV luminescent organic-capped ZnO quantum dots synthesized by alkoxide hydrolysis with dilute water, J. Colloid Interface Sci. 355 (2011) 274–281.
[28] N. Tsubokawa, Surface grafting of polymers onto nanoparticles in a solvent-free dry-system and applications of polymer-grafted nanoparticles as novel functional hybrid materials, Polym. J. (Tokyo, Jpn.) 39 (2007) 983–1000.
[29] A. Kołodziejczak-Radzimska, T. Jesionowski, Zinc oxide—from synthesis to application: a review, Materials. 7 (2014) 2833.
[30] F. Bertrand, S.-A. German, A. Anwar, V. Irune, B. Gemma, R.D.M. Yolanda, B. Lennart, Dispersion and surface functionalization of oxide nanoparticles for transparent photocatalytic and UV-protecting coatings and sunscreens, Sci. Technol. Adv. Mater. 14 (2013) 023001–023023.
[31] L. Brus, Electronic wave functions in semiconductor clusters: experiment and theory, J. Phys. Chem. 90 (1986) 2555–2560.
[32] Y.C. Kong, D.P. Yu, B. Zhang, W. Fang, S.Q. Feng, Ultraviolet-emitting ZnO nanowires synthesized by a physical vapor deposition approach, Appl. Phys. Lett. 78 (2001) 407–409.
[33] A. van Dijken, E.A. Meulenkamp, D. Vanmaekelbergh, A. Meijerink, The luminescence of nanocrystalline ZnO particles: the mechanism of the ultraviolet and visible emission, J. Lumin. 87–89 (2000) 454–456.
[34] M. Sato, A. Kawata, S. Morito, Y. Sato, I. Yamaguchi, Preparation and properties of polymer/zinc oxide nanocomposites using functionalized zinc oxide quantum dots, Eur. Polym. J. 44 (2008) 3430–3438.
[35] B. Guo, Z.R. Qiu, K.S. Wong, Intensity dependence and transient dynamics of donor-acceptor pair recombination in ZnO thin films grown on (001) silicon, Appl. Phys. Lett. 82 (2003) 2290–2292.
[36] S.A. Studenikin, N. Golego, M. Cocivera, Fabrication of green and orange photoluminescent, undoped ZnO films using spray pyrolysis, J. Appl. Phys. 84 (1998) 2287–2294.
[37] S. Repp, S. Weber, E. Erdem, Defect evolution of nonstoichiometric ZnO quantum dots, J. Phys. Chem. C 120 (2016) 25124–25130.
[38] H. Waqas, M.S. Salman, A. Riaz, N. Riaz, S. Shabbir, Unique morphologies of zinc oxide synthesized by thermal decomposition and co-precipitation routes: ultraviolet absorption and luminescence characteristics, Cryst. Res. Technol. 50 (2015) 379–388.
[39] D. Liu, Y.H. Lv, M. Zhang, Y.F. Liu, Y.Y. Zhu, R.L. Zong, Y.F. Zhu, Defect-related photoluminescence and photocatalytic properties of porous ZnO nanosheets, J. Mater. Chem. A 2 (2014) 15377–15388.
[40] P. Camarda, L. Vaccaro, F. Messina, M. Cannas, Oxidation of Zn nanoparticles probed by online optical spectroscopy during nanosecond pulsed laser ablation of a Zn plate in H_2O, Appl. Phys. Lett. 107 (2015) 013103.
[41] F. Fabbri, M. Villani, A. Catellani, A. Calzolari, G. Cicero, D. Calestani, G. Calestani, A. Zappettini, B. Dierre, T. Sekiguchi, G. Salviati, Zn vacancy induced green luminescence on non-polar surfaces in ZnO nanostructures, Sci Rep 4 (2014) 5158.
[42] C. Klingshirn, ZnO: from basics towards applications, Phys. Status Solidi B 244 (2007) 3027–3073.
[43] C. Klingshirn, ZnO: material, physics and applications, ChemPhysChem 8 (2007) 782–803.
[44] P. Camarda, F. Messina, L. Vaccaro, S. Agnello, G. Buscarino, R. Schneider, R. Popescu, D. Gerthsen, R. Lorenzi, F.M. Gelardi, M. Cannas, Luminescence mechanisms of defective ZnO nanoparticles, Phys. Chem. Chem. Phys. 18 (2016) 16237–16244.
[45] M. Wang, E.K. Na, J.S. Kim, E.J. Kim, S.H. Hahn, C. Park, K.K. Koo, Photoluminescence of ZnO nanoparticles prepared by a low-temperature colloidal chemistry method, Mater. Lett. 61 (2007) 4094–4096.
[46] P. Kumbhakar, D. Singh, C.S. Tiwary, A.K. Mitra, Chemical synthesis and visible photoluminescence emission from monodispersed ZnO nanoparticles, Chalcogenide Lett. 5 (2008) 387–394.
[47] Z.G. Zang, M.Q. Wen, W.W. Chen, Y.F. Zeng, Z.Q. Zu, X.F. Zeng, X.S. Tang, Strong yellow emission of ZnO hollow nanospheres fabricated using polystyrene spheres as templates, Mater. Des. 84 (2015) 418–421.
[48] L. Guo, S.H. Yang, C.L. Yang, P. Yu, J.N. Wang, W.K. Ge, G.K.L. Wong, Highly monodisperse polymer-capped ZnO nanoparticles: preparation and optical properties, Appl. Phys. Lett. 76 (2000) 2901–2903.
[49] K. Borgohain, S. Mahamuni, Luminescence behaviour of chemically grown ZnO quantum dots, Semicond. Sci. Technol. 13 (1998) 1154–1157.
[50] H.M. Xiong, D.P. Liu, Y.Y. Xia, J.S. Chen, Polyether-grafted ZnO nanoparticles with tunable and stable photoluminescence at room temperature, Chem. Mater. 17 (2005) 3062–3064.
[51] H.P. Wang, H. Jiang, X.M. Wang, Construction of strong alkaline microcavities for facile synthesis of fluorescence-tunable ZnO quantum dots, Chem. Commun. 46 (2010) 6900–6902.
[52] H.M. Xiong, D.P. Xie, X.Y. Guan, Y.J. Tan, Y.Y. Xia, Water-stable blue-emitting ZnO@polymer core-shell microspheres, J. Mater. Chem. 17 (2007) 2490–2496.
[53] M. Abdullah, T. Morimoto, K. Okuyama, Generating blue and red luminescence from ZnO/poly(ethylene glycol) nanocomposites prepared using an in-situ method, Adv. Funct. Mater. 13 (2003) 800–804.
[54] M. Hood, M. Mari, R. Muñoz-Espí, Synthetic strategies in the preparation of polymer/inorganic hybrid nanoparticles, Materials 7 (2014) 4057.
[55] W. Zheng, R. Ding, X. Yan, G. He, PEG induced tunable morphology and band gap of ZnO, Mater. Lett. 201 (2017) 85–88.
[56] X.M. Peng, Y.W. Chen, F. Li, W.H. Zhou, Y.H. Hu, Preparation and optical properties of ZnO@PPEGMA nanoparticles, Appl. Surf. Sci. 255 (2009) 7158–7163.
[57] Y.L. Wu, A.I.Y. Tok, F.Y.C. Boey, X.T. Zeng, X.H. Zhang, Surface modification of ZnO nanocrystals, Appl. Surf. Sci. 253 (2007) 5473–5479.
[58] S. Tachikawa, A. Noguchi, T. Tsuge, M. Hara, O. Odawara, H. Wada, Optical properties of ZnO nanoparticles capped with polymers, Materials 4 (2011) 1132–1143.
[59] H.M. Xiong, Z.D. Wang, Y.Y. Xia, Polymerization initiated by inherent free radicals on nanoparticle surfaces: a simple method of obtaining ultrastable (ZnO)polymer core-shell nanoparticles with strong blue fluorescence, Adv. Mater. 18 (2006) 748–751.
[60] F. Piersimoni, R. Schlesinger, J. Benduhn, D. Spoltore, S. Reiter, I. Lange, N. Koch, K. Vandewal, D. Neher, Charge transfer absorption and emission at ZnO/organic interfaces, J. Phys. Chem. Lett. 6 (2015) 500–504.